A WEARABLE ACTIVE GPS ANTENNA FOR APPLICATION IN SMART TEXTILES

Dierck, A., De Keulenaer, T., Declercq, F., and Rogier, H.

Department of Information Technology, Ghent University, 9000 Ghent, Belgium

ABSTRACT

This paper describes the design of a wearable, active Global Positioning System antenna for application in smart textiles. The antenna is a circularly polarized aperture-coupled microstrip-patch antenna for use in the L1-band at 1.57542 GHz. A quadrature hybrid coupler was used to obtain right-handed circular polarization. A low-noise amplifier was integrated onto the backside of the microstrip patch antenna. A gain of 5 dBi was measured for the passive radiator, whereas the measured low-noise amplifier available gain is 18.1 dB. When integrating the two components into a single active antenna, this results in a combined gain of 23.6 dBi.

Key words: aperture coupled microstrip patch antenna, wearable, circular polarization, active, GPS, smart textiles, low noise amplifier, LNA.

1. INTRODUCTION

For space, aeronautical and terrestrial communications, there is a need for low-weight, flexible Smart Fabrics, Interactive Textile (SFIT) electronic systems that are unobtrusively integrated into garments, without disturbing the comfort or the movements of the wearer. Given its size, the wearable antenna forms a vital component in such a system. The last decades, research on textile antennas has boomed and many robust textile antennas have been proposed that exhibit efficient radiation characteristics under many adverse conditions such as antenna bending or moisture [2]-[16]. For example, in [3] and [4], respectively, a textile GPS antenna and a textile 2.45 GHz off-body communication antenna for integration into protective firefighter clothing are presented. In [2], a textile antenna array and its integration into a space suit is discussed. In most of the cited works, however, the antenna consists of a patch fed by a coaxial probe-feed. The via implementing the probe feed adds to the rigidity of the flexible antenna and poses a weak link in the connection between the wearable antenna and the transceiver when exposed to extreme movements, such as performed by rescue workers during an intervention. Therefore, in this contribution a more robust solution is presented by integrating an active electronic system directly underneath the textile patch antenna [15] and by using aperture coupling as a feeding technique [8] instead of a coaxial feed. Additionally, to provide even more robustness, a discrete quadrature hybrid coupler is used to realize circular polarization, as opposed to e.g. asymmetries in the patch [3] [4]. Specifically, in this contribution an active GPS antenna is presented. The intended application is in the area of smart textiles, so an aperture-coupled patch antenna was chosen because of its low profile and its potential to be implemented using flexible materials. On the antenna backside, a low-noise amplifier (LNA) is integrated with the patch feed structure. Aiming at GPS reception in the L1-band, a right-handed circular polarization pattern is required in a 2.046 MHz wide band centered around 1.57542 GHz, preferably covering a wide range of elevation angles. A discrete quadrature hybrid coupler [20] was used to obtain circular polarization. After simulation, the antenna was built using very thin flexible copper-on-polyimide films for the patch, ground plane/aperture and feed structure/LNA layer. In between these layers, aramid and protective polyurethane foam were used as dielectric material. The manufactured antennas were then measured and compared to the simulations. The antenna design is presented in Section 2. The design of the LNA is discussed in Section 3. Section 4 presents the measured antenna and LNA characteristics.

2. ANTENNA DESIGN

2.1. Material selection

As shown in Fig. 1, the active aperture coupled patch antenna consists of an antenna substrate and a feed substrate. For the antenna substrate, a polyurethane foam called Urecom® from Recticel was chosen. The feed substrate was made out of aramid. The antenna substrate material is thicker than the feed substrate material and has a lower ϵ_r, as to ensure high radiation efficieny by the patch antenna, in the meanwhile keeping radiation from the feed structure and LNA low. The characteristics of the substrates are shown in Tab. 1. The antenna patch, feed lines and ground plane with slots are etched in a flexible copper-on-polyimide film, UPISEL®-N by UBE [18]. The thickness of the copper layer in this laminate is 9 µm, while the polyimide layer has a thickness of 25 µm. A cross-section visualizing the different material layers is

shown in Fig. 2. The different layers were assembled using a thermally activated adhesive by means of alignment holes etched in the copper-on-polyimide film.

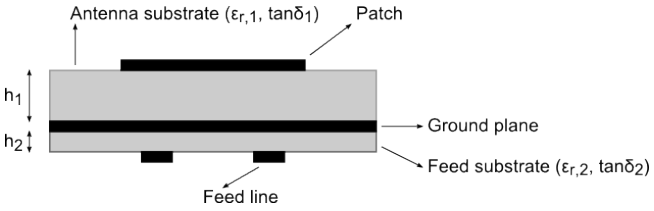

Figure 1. Layer structure of the GPS antenna

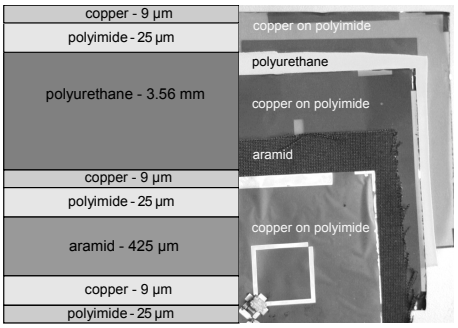

Figure 2. Material layers

Table 1. Properties of feed and antenna substrate

Substrate	Feed	Antenna
Material	aramid	polyurethane
ϵ_r	1.99	1.25
tanδ	0.016	0.015
h	0.40 mm	3.56 mm

2.2. Antenna geometry

The realized antenna geometry consists of a square patch, a ground plane with two slots and a feed line for each slot forming a 90° bend to accommodate the quadrature hybrid coupler, as shown in Fig. 3. Each slot is aligned to the middle of the edge on which it creates a radiating mode. Aperture coupling was chosen to avoid the use of vias through the polyurethane, augmenting the robustness and flexibility of the antenna. The center position of the slots allows for a strong excitation of two orthogonal modes on the patch, whereas the quadrature hybrid coupler produces a 90° phase difference between the modes over a wide frequency range. The realization of this phase difference by means of a discrete component, as opposed to phase difference generation by means of e.g. asymmetries in the microstrip patch/feed structure, ensures its robustness, as it provides circular polarization within a large frequency band.

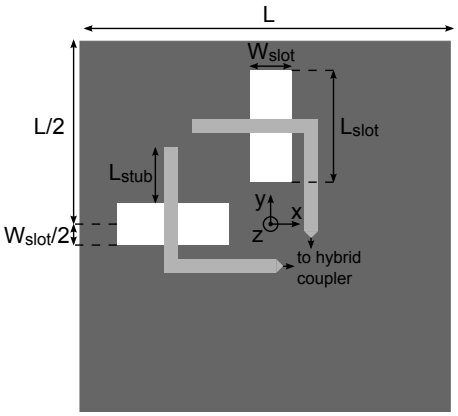

Figure 3. Geometry of the GPS antenna

2.3. Antenna design

The antenna design was carried out by imposing criteria for the return loss $|S_{11}|$ and the axial ratio AR. Since the antenna structure is symmetric, only the return loss of one feed line was optimized during design. It is, however, important to ensure that the coupling between the two feed lines is low, so that the power is indeed delivered to the antenna for radiation. The antenna simulations were carried out in the ADS Momentum 2.5D environment. The final antenna dimensions are specified in Tab. 2, its $|S_{11}|$, gain and axial ratio are shown in Fig. 4. It is seen that the $|S_{11}|$ at 1.575 GHz is lower than -17 dB, the gain is 7 dBi and the axial ratio is 1.74 dB. The 3 dB beam width and 3 dB AR beam width are both larger than 70°. It must be noted that the discrete quadrature hybrid coupler was not included in the simulation, but the 90° phase difference was imposed in the ADS Momentum post processing. Therefore, we expect to see a lower gain in the real-life prototypes, as the passive quadrature hybrid exhibits 3 dB insertion loss.

Table 2. Final antenna dimensions

Parameter	Size(mm)
L	75.25
L_{stub}	16.80
L_{slot}	23.00
W_{slot}	4.20

3. LNA DESIGN

3.1. LNA topology

The LNA was built around an Avago ATF-54143 pHEMT transistor, using a grounded-source topology [1]. The LNA layout including active and passive components is shown in Fig. 5. A 3 V DC voltage can be supplied via a solder pad or via the output UFL connector, where the $\lambda/4$ microstrip transmission line TL4 in combination

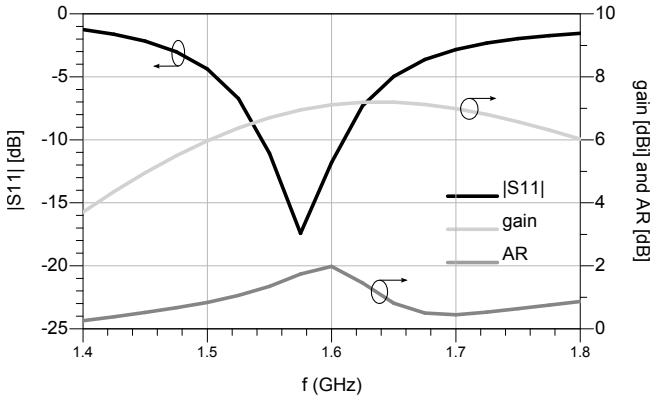

Figure 4. Simulated gain, axial ratio and $|S_{11}|$

with C10 forms a high impedance at the working frequency between the output and the 3 V bias pad. L2 and C9 provide additional AC blocking. The transistor gate is biased via the resistive voltage divider R3-R4 through the inductor L1. Bias to the drain is provided via the $\lambda/4$ microstrip transmission line TL3 in combination with capacitor C8. R1 provides a resistive termination at low frequencies, enhancing stability. R2 limits the gate current at high input power. Resistor R5 provides stability below 5 GHz. At higher frequencies stability is ensured by providing a low impedance connection between source and ground. In- and output matching are realized by capacitor-stub-capacitor filters formed by C1-TL1-C2 and C6-TL2-C7.

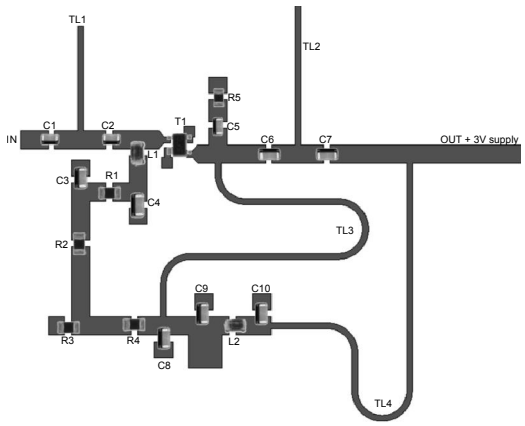

Figure 5. LNA circuit

3.2. LNA design

The criteria imposed for the LNA design were a high gain, good in- and output matching and, of course, a low noise figure. Since the LNA is placed in-between two 50 Ω terminated devices and its in- and output will be matched to 50 Ω, the $|S_{21}|$ can be used as a gain measure. In- and output matching are performed using matching networks, imposing a $<$ -10 dB condition on both the $|S_{11}|$ and $|S_{22}|$. As for the noise figure, we aimed at a value around 0.5 dB. Stability was taken into account by means of the stability factor K and the stability measure B_1 [21]. For unconditional stability, the K factor should be larger than 1 while the stability measure should be positive. The passive LNA interconnections and transmission lines were simulated in the ADS Momentum 2.5D environment, while the discrete active and passive components were simulated in the ADS circuit simulator. The final components are listed in Tab. 3. The capacitors are 0603 SMD parts from Murata and Johanson Technology, the coils are 0603 SMD parts from Coilcraft. The simulation results will be discussed in section 4.2, where they will be compared with the measurement results.

Table 3. Used components and their values

Component	Value	Component	Value
C1	30 pF	R1	50 Ω
C2	4.7 pF	R1	1 kΩ
C3	220 pF	R1	330 Ω
C4,C5	6.8 pF	R1	1.8 kΩ
C6	10 pF	R1	120 Ω
C7	22 pF	L1,L2	10 nH
C8	12 pF	TL1	9.5 mm
C9	100 nF	TL2	12.75 mm
C10	12 pF	TL3,TL4	41.5 mm

3.3. Optional SAW filter

In the final layouts, the possibility to include an SAW filter at the LNA input was provided. The EPCOS B-9080 SAW filter was chosen [19]. This is a low insertion loss L1 band pass filter and provides additional signal suppression of out-of-band signals, such as DAB between 1.452 GHz and 1.492 GHz or cellular signals in the DCS-1800 band. The LNA with SAW was not simulated, as no simulation data was available for the SAW filter.

4. MEASUREMENTS

A passive and active version of the antenna were fabricated, as well as a standalone version of the LNA, as to measure the characteristics of the antenna and LNA on their own and compare these to the measurement results of the active antenna. The LNA and active antenna were fabricated in two versions: with and without SAW filter. Pictures of the active antenna prototype with SAW filter are shown in Fig. 6 and Fig. 7. The measurements were performed using the N5242 A PNA-X Vector Network Analyzer from Agilent Technologies.

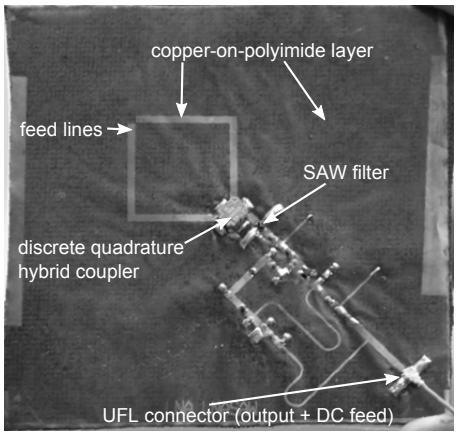

Figure 6. Picture of the antenna backside with LNA

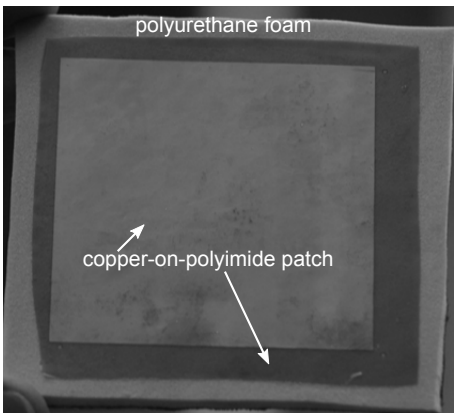

Figure 7. Picture of the antenna front

4.1. Antenna measurements

The radiation pattern of the passive antenna was measured in both the XZ and the YZ plane, using a standard gain horn in the anechoic chamber. Measurements were also performed for an antenna covered by aramid, to analyze the effect of integration into a textile garment. The aramid layer had no noticeable influence on the antenna characteristics. The radiation patterns of the active antenna were similar. The XZ and YZ patterns of the aramid covered passive antenna are shown in Fig. 8 and 9. The antenna gain at 0° is 5 dBi. The gain, axial ratio and $|S_{11}|$ as a function of the frequency are shown in Fig. 10. When we compare this with the simulated results from Fig. 4, we clearly notice the effect of the discrete quadrature hybrid coupler, more specifically the broad 50 Ω match. The measured AR curve also behaves differently, providing a 3 dB axial ratio bandwidth that is less broadband than simulated. However, the 3 dB AR bandwidth remains sufficiently broad for GPS L1 operation. At 1.575 GHz, the AR is 2.2 dB, which is higher than simulated, but still well below 3 dB. The 3 dB beam width and 3 dB AR beam width are both larger than 70°.

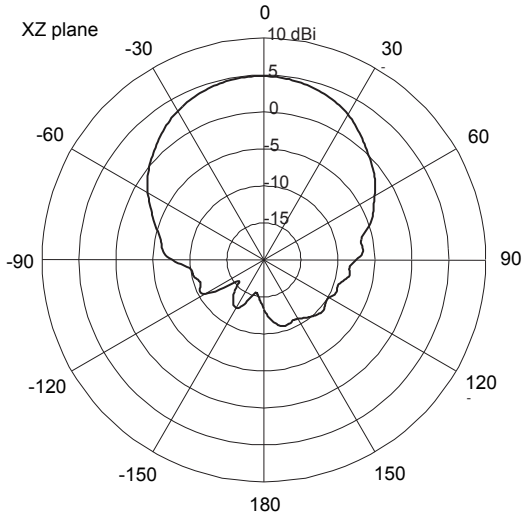

Figure 8. Radiation pattern of the aramid covered passive antenna in the XZ plane

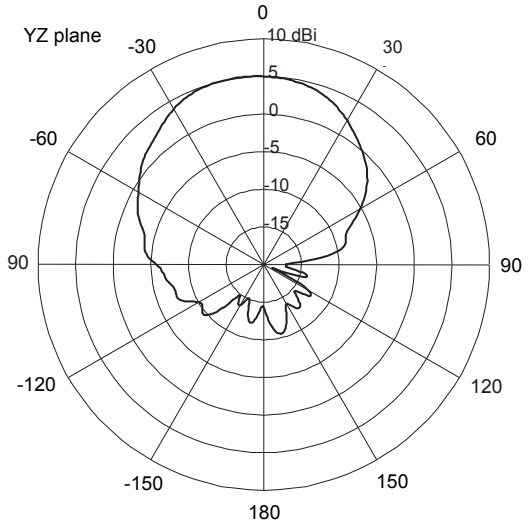

Figure 9. Radiation pattern of the aramid covered passive antenna in the YZ plane

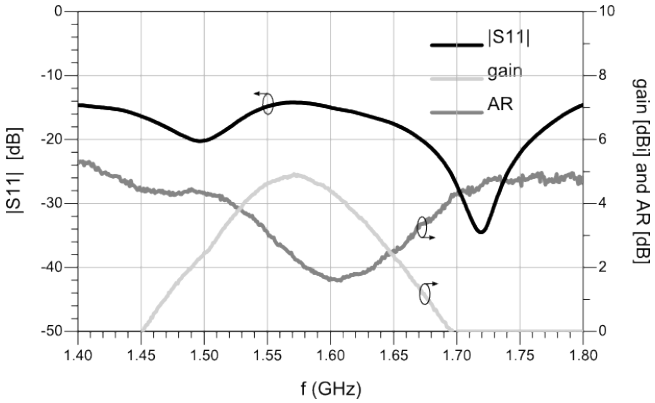

Figure 10. Measured gain, axial ratio and $|S_{11}|$ of the passive antenna

4.2. LNA measurements

The two-port scattering parameters and noise figure of the LNA were measured both with and without SAW filter. From the measured S-parameters, K factor and stability measure B_1 were calculated.

4.2.1. LNA without SAW filter

Measurement and simulation results of the LNA without SAW filter are shown in Fig. 11 to 13. The measured $|S_{21}|$ at the L1 band center frequency is in good agreement with the simulated value, both being about 18.1 dB. The measured noise figure, being 0.545 dB, is also in good agreement with the simulated value, which was 0.475 dB. Both measured and simulated $|S_{12}|$ (not shown in on graphs) are well below -20 dB. Less agreement is found between the measured and simulated $|S_{11}|$ and $|S_{22}|$. The measured curves seem to be shifted upwards to the right, all the more so for $|S_{11}|$. At the L1 band center frequency, the measured $|S_{22}|$ is still comparable to the simulated value and lower than -10 dB. The measured $|S_{11}|$ at this frequency, however, differs greatly from the simulated value, and exceeds -10 dB. An explanation could be found in the difference between the simulation and the measurement setup. During measurements, the LNA was interfaced by means of UFL connectors and cables. These were not taken into account during the simulation. Comparing the stability of the simulated and the measured LNA, it is seen that the measured stability factor K drops below 1 between 1 and 1.7 GHz, so unconditional stability in that frequency range is not ensured. However, no instability was encountered during measurements and connection to a GPS receiver. The measured LNA power consumption is 84 mW.

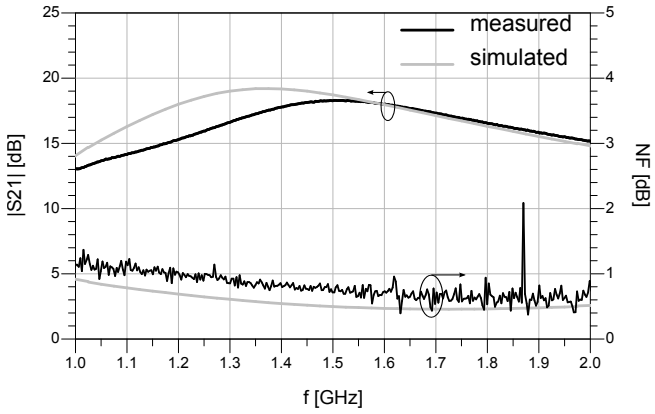

Figure 11. Simulated and measured LNA $|S_{21}|$ and noise figure

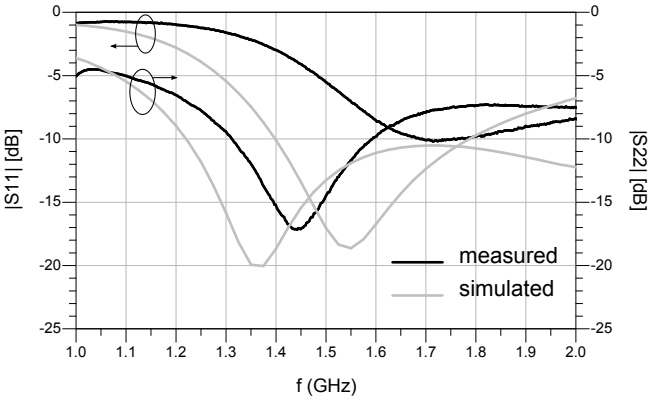

Figure 12. Simulated and measured LNA $|S_{11}|$ and $|S_{22}|$

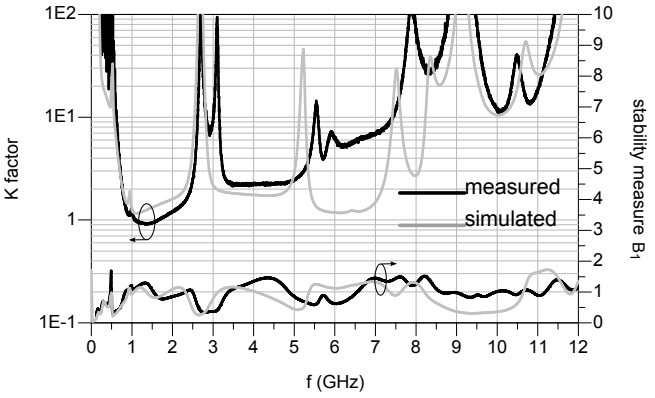

Figure 13. Simulated and measured LNA K factor and stability measure

4.2.2. LNA with SAW filter

Measurement results of the LNA with SAW filter are shown in Fig. 14 to 16. The effect of the SAW filter is clearly visible in the results, which show that the operation of the LNA is limited to the SAW filter pass band. The $|S_{21}|$ and noise figure differ from the values for the LNA without SAW filter by about 1.5 dB, i.e. the insertion loss of the SAW filter. The $|S_{11}|$ and $|S_{22}|$ are within specifications, being less than -10 dB. The K factor and stability measure indicate that unconditional stability is guaranteed from 0 to 12 GHz.

4.3. Active antenna measurements

The gain, axial ratio and $|S_{11}|$ as a function of frequency for the active antenna with and without SAW filter are shown in Fig. 17 and Fig. 18. The total gain, consisting of the antenna and LNA gain, in the main radiation direction is 23.6 dB for the active antenna without SAW filter and 21.5 dB for the active antenna with SAW filter, which could be expected from the separate antenna and LNA measurements. The AR of the antenna without SAW has the same behavior as the passive antenna's AR. It is, however, about 1 dB lower. This could be caused

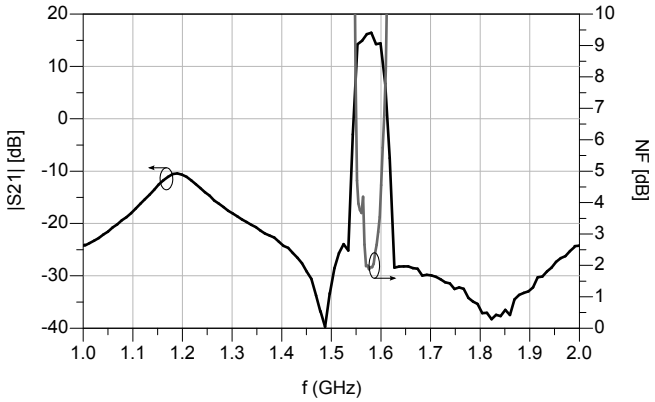

Figure 14. Measured LNA with SAW $|S_{21}|$ and noise figure

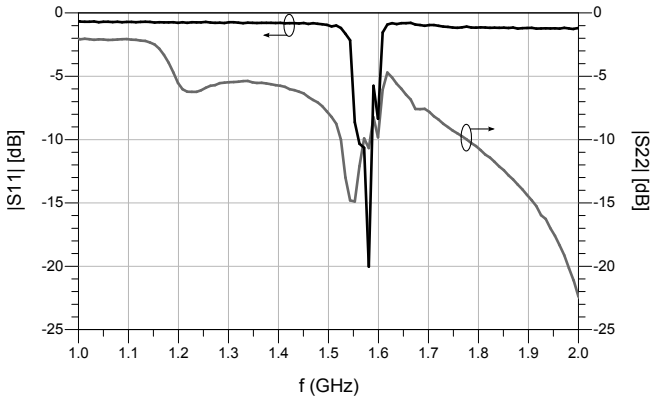

Figure 15. Measured LNA with SAW $|S_{11}|$ and $|S_{22}|$

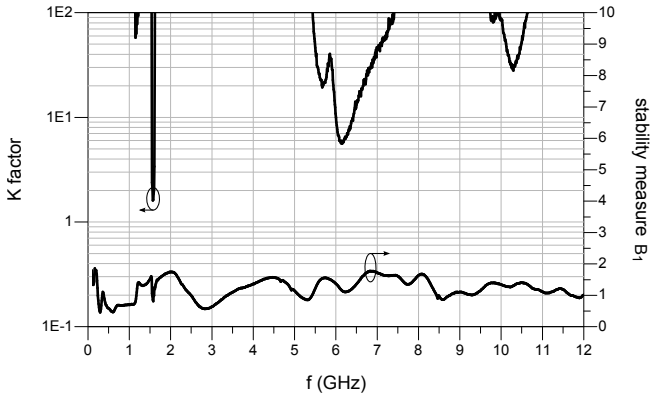

Figure 16. Measured LNA with SAW K factor and stability measure

by small differences originating from the alignment process. The AR characteristic of the active antenna with SAW filter differs from the one without SAW. The bandpass nature of the SAW filter is clearly visible. The $|S_{11}|$ of the antenna without SAW is -9 dB. The $|S_{11}|$ of the antenna with SAW filter is -9.5 dB. Both antennas achieve a 3 dB beam width and a 3 dB AR beam width larger than 70°.

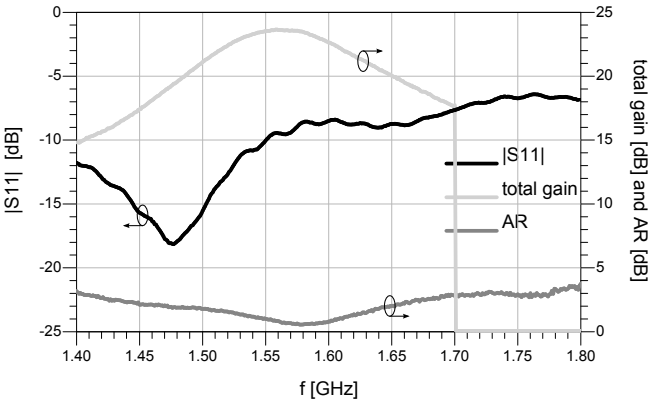

Figure 17. Measured gain, axial ratio and $|S_{11}|$ of the active antenna without SAW filter

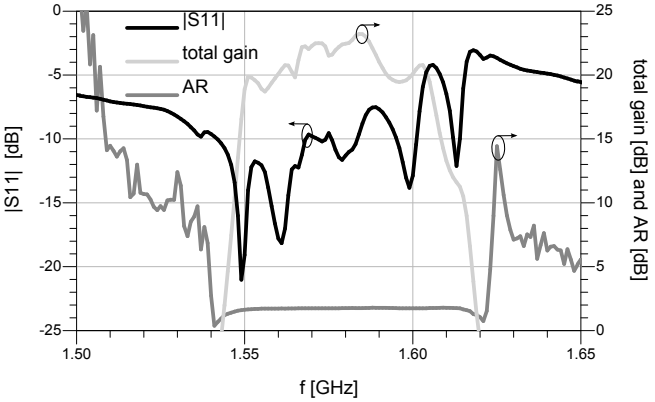

Figure 18. Measured gain, axial ratio and $|S_{11}|$ of the active antenna with SAW filter

5. CONCLUSIONS

The presented active antenna is able to cover the 2.042 MHz wide GPS L1 band at 1.57542 GHz with a combined antenna and LNA gain of 23.6 dB, a noise figure of 0.5 dB, an axial ratio of 0.7 dB and an $|S_{11}|$ of -9 dB for the antenna without SAW filter. The active antenna weight is 14 g. Upon connection of the active antenna to a GPS receiver, it provided us with better carrier to noise ratios than the off-the-shelf rigid active antenna provided alongside the receiver.

REFERENCES

[1] A.J.Ward, AN-1222 High Intercept Noise Amplifier for the 1850 - 1910 MHz PCS Band using the Agilent ATF-54143 Enhancement Mode PHEMT, Agilent Technologies, 2006.

[2] T.F. Kennedy, P.W. Fink, A.W. Chu, N.J. Champagne II, G.Y. Lin, M.A. Khayat, Body-worn E-textile Antennas: The Good, the Low-Mass, and the Conformal, IEEE Transactions on Antennas and Propagations, Vol. 57, No.4, April, 2009

[3] L. Vallozzi, W. Vandendriessche, H. Rogier, C. Hertleer, and M. Scarpello, Design of a Protective Garment GPS-Antenna, Microwave and Optical Technology Letters, Vol. 51, No.6, June, 2009

[4] C. Hertleer, H. Rogier, L. Vallozzi, and L. Van Langenhove, A Textile Antenna for Off-Body Communication Integrated Into Protective Clothing for Firefighters, IEEE Transactions on Antennas and Propagations, Vol. 57, No.4, April, 2009

[5] P. Salonen, Y. Rahmat-Samii, Textile Antennas: Effects of Antenna Bending on Input Matching and Impedance Bandwidth, IEEE A&E Systems Magazine, March 2007

[6] Q. Bai, R.J. Langley, Effect of Bending and Crumpling on Textile Antennas, 2nd IET Seminar on Antennas and Propagation for Body-Centric Wireless Communications, 2009

[7] A. Tronquo, H. Rogier, C. Hertleer, and L. Van Langenhove, A Robust Planar Textile Antenna for Wireless Body LANs Operating in the 2.45-GHz ISM band, IEE Electronics Letters, vol. 42, no. 3, pp. 142-143, Feb. 2006.

[8] C. Hertleer, A. Tronquo, H. Rogier, L. Vallozzi, and L. Van Langenhove, Aperture-Coupled Patch Antenna for integration into wearable textile systems, IEEE Antennas and Wireless Propagation Letters, vol. 6, pp. 392-395, 2007.

[9] C. Hertleer, A. Tronquo, H. Rogier, and L. Van Langenhove, The Use of Textile Materials to Design Wearable Microstrip Patch Antennas, Textile Research Journal, vol. 78, no. 8, pp. 651-658, Aug. 2008.

[10] L. Vallozzi, H. Rogier, and C. Hertleer, Dual Polarized Textile Patch Antenna for Integration into Protective Garments, IEEE Antennas and Wireless Propagation Letters, vol. 7, pp. 440-443, 2008.

[11] C. Hertleer, A. Van Laere, H. Rogier, L. Van Langenhove, Influence of Relative Humidity on Textile Antenna Performance, Textile Research Journal, vol. 80, no. 2, pp. 177-183, Jan. 2010.

[12] P. Van Torre, L. Vallozzi, C. Hertleer, H. Rogier, M. Moeneclaey, J. Verhaevert, Indoor off-body communication by means of a textile multiantenna system integrated in clothing for rescue workers, IET Science, Measurement & Technology, vol. 4, no. 2 , p. 41-52, Mar. 2010.

[13] L. Vallozzi, P. Van Torre, C. Hertleer, H. Rogier, M. Moeneclaey, J. Verhaevert, Wireless communication for firefighters using dual-polarized textile antennas integrated in their garment, IEEE Trans. on Antennas Propag., vol. 58, no.4, pp. 1357-1368, Apr. 2010.

[14] C. Hertleer, L. Van Langenhove and H. Rogier, Flexible textile-based antennas for off-body communication of a wearable textile system, Materials Technology, vol. 25, no.2, pp. 101-105, Jul. 2010.

[15] F. Declercq and H. Rogier, Active Integrated Wearable Textile Antenna with Optimized Noise Characteristics, IEEE Trans. on Antennas Propag., accepted for publication, June 2009.

[16] P. Van Torre, L. Vallozzi, H. Rogier, M. Moeneclaey, C. Hertleer, J. Verhaevert, Indoor off-body wireless MIMO communication with dual polarized textile antennas, IEEE Trans. on Antennas Propag., accepted for publication, Dec. 2009.

[17] T. De Keulenaer, A. Dierck, Ontwerp van een actieve GPS-antenna voor toepassing in intelligent textiel, Master Thesis, 2010.

[18] UBE UPISEL®-N datasheet, http://www.ube.es/archivos/pdfs/UpiselN-567.pdf.

[19] EPCOS B9080 datasheet, http://www.epcos.com/inf/40/ds/mc/B9080.pdf.

[20] Anaren XC1400P-03S datasheet http://www.anaren.com/Content/File/Product/XC1400P-03S%20Data%20Sheet%20Rev%20B.pdf

[21] R. Gilmore, L. Besser, Practical RF Circuit Design for Modern Wireless Systems - Volume II - Active Circuits and Systems, Artech House.